Energy Reports 8 (2022) 10762–10775

Contents lists available at ScienceDirect

Energy Reports

journal homepage: www.elsevier.com/locate/egyr

Research Paper

Novel active management of compressive pressure on a lithium-ion battery using a phase transition actuator

Jinho Jeong [a], Eunji Kwak [a], Jun-hyeong Kim [a], Ki-Yong Oh [a,b,*]

[a] Department of Mechanical Convergence Engineering, Hanyang University, 222 Wangsimni-ro, Seongdong-gu, Seoul, 04763, Republic of Korea
[b] School of Mechanical Engineering, Hanyang University, 222 Wangsimni-ro, Seongdong-gu, Seoul, 04763, Republic of Korea

ARTICLE INFO

Article history:
Received 6 June 2022
Received in revised form 10 August 2022
Accepted 13 August 2022
Available online xxxx

Keywords:
Active pressure management
Health management
Lithium-ion battery
Phase transition actuator

ABSTRACT

This study proposes a novel method for managing the compressive pressure imposed on a lithium-ion battery (LIB) using a phase transition actuator under constrained conditions considering the influence of compressive pressure on the performance and lifespan of LIBs. Specifically, an active pressure management strategy is proposed to maintain the optimal pressure and reduce the equivalent impedance during operation. A closed-loop control scheme is used to maintain compressive pressure via a phase transition actuator considering the dynamic characteristics of the actuator. This configuration allows managing both reversible pressure due to phase transitions at lithium intercalation/deintercalation and irreversible pressure evolution due to solid–electrolyte interface formation and growth. The analysis on experiments indicates that the equivalent impedance and capacity can be managed through active pressure management under stationary and stochastic operational conditions, demonstrating the effectiveness of the proposed method. Specifically, the accumulated stress in an LIB caused by pressure variation is reduced by 56.17% under a stochastic load condition when activating the proposed pressure management strategy, resulting in a 1.47% increase in discharge capacity immediately after operation compared to that under a passive pressurized condition. The proposed method is simple, effective, and economically feasible for battery management systems in terms of compression pressure control.

1. Introduction

Lithium-ion batteries (LIBs) have recently been highlighted as indispensable energy storage systems for not only laptops and mobile phones, but also automobiles and energy storage systems based on their high energy density, high power density, and low self-discharge characteristics (Manthiram, 2011). To extend the territory of LIB applications, intensive studies have been conducted on the improvement of LIB performance and lifespan (Costa et al., 2021; Beirão et al., 2016; Zhang et al., 2014). In particular, studies on the lifespan of LIBs are directly correlated to the replacement schedule of LIBs, suggesting that the total cost of operation of LIBs can be reduced through novel health management strategies.

Many efforts have been devoted to studying the effects of operational environments, including depth of discharge (Käbitz et al., 2013; Ecker et al., 2014), charge and discharge rate (Keil and Jossen, 2016), and temperature (Jalkanen et al., 2015; Waldmann et al., 2014), on LIB characteristics and degradation. The effects of compressive pressure on LIBs have received significant attention because compressive pressure is highly correlated to LIB characteristics and lifespan. Specifically, compressive pressure can modify the initiation and growth of dendrites, thereby smoothing surfaces and eliminating voids on the atomic scale (Fang et al., 2021; Shen et al., 2021; Zhang et al., 2019). Therefore, applying appropriate compressive pressure to an LIB is effective at reducing contact impedance between the electrode and current collector (Müller et al., 2019a; Dsoke et al., 2013; Berckmans et al., 2019). However, excessive pressure causes deformation of the electrodes and separator, and interferes with the transportation of lithium ions, adversely affecting LIB characteristics and lifespan.

Strong correlation between compressive pressure and LIB dynamic characteristics suggests that an optimal compressive pressure should be applied to LIBs, particularly for applications in electric vehicles (EVs), in that LIB modules and packs are exposed to harsh environmental conditions. This correlation has also motivated many studies focusing on long-term experiments at different pressures (Cannarella and Arnold, 2014a,b; Barai et al., 2017), revealing that LIBs undergo a volume change (i.e., swelling) based on two phenomena during operation. First, reversible swelling caused by the phase transition of active materials induces periodic pressure evolution under constrained conditions (Zhang

* Corresponding author at: Department of Mechanical Convergence Engineering, Hanyang University, 222 Wangsimni-ro, Seongdong-gu, Seoul, 04763, Republic of Korea.
E-mail address: kiyongoh@hanyang.ac.kr (K.-Y. Oh).

https://doi.org/10.1016/j.egyr.2022.08.198

Nomenclature

Abbreviation

BMS	Battery management system
CC	Constant current
CCCV	Constant current constant voltage
EIS	Electrochemical impedance spectroscopy
EV	Electric vehicle
LIB	Lithium-ion battery
LFP	Lithium iron phosphate
NMC	Lithium nickel manganese cobalt oxide
RMSE	Root-mean-squared-error
SEI	Solid electrolyte interface
SOC	State of charge

Symbols

k_B	Stiffness of battery
$P_{initial}$	Pressure due to initial constraint
$P_{swelling}$	Pressure due to charging

Greek letters

δ_i	Deformation displacement due to initial constraint
δ_s	Free swelling displacement due to charging

and Tang, 2012; Wang et al., 2007; Siegel et al., 2013). The variation of reversible pressure originates from changes in the microscopic molecular structures of active materials based on the movement and diffusion of lithium ions during charge and discharge, which causes macroscopic changes in LIB volume. The accumulated stress associated with reversible pressure variation causes mechanical fatigue, resulting in performance degradation, including capacity loss and eventual failure (Sethuraman et al., 2010, 2012; Mukhopadhyay et al., 2012; Kaasik et al., 2013; Shi et al., 2011; Peabody and Arnold, 2011). Specifically, graphite anodes play a significant role in swelling under unconstrained conditions and swelling-induced pressure under constrained conditions. Second, irreversible swelling caused by the formation and growth of a solid–electrolyte interface (SEI) layer results in pressure evolution under constrained conditions (Bitzer and Gruhle, 2014; Cannarella and Arnold, 2014b; Louli et al., 2019). This phenomenon is attributed to the formation and growth of cracks on the surface of the anode, resulting in SEI formation, gas generation, and lithium plating during operation (Vetter et al., 2005; Kotak et al., 2018). These two phenomena indicate that the optimal pressure set initially cannot be maintained during short-term operation and excessive pressure will be imposed on LIBs during long-term operation, which adversely affects LIB characteristics and lifespan. Therefore, the stress caused by mechanical evolution from these two sources is strongly correlated with the management of LIB lifespan. Several studies have also been conducted to model these phenomena using phenomenological modeling (Oh et al., 2016) or machine learning methods (Kwak et al., 2021).

To ensure optimal performance and prolong the lifespan of LIBs, LIBs should be operated under optimal pressure conditions. Some studies have been conducted on passive pressure management by applying an initial optimal pressure to LIBs (Müller et al., 2019b; Zhang et al., 2020). The passive management of compression pressure can reduce equivalent impedance under initial operational conditions. However, the formation and growth of an SEI result in irreversible volume changes in LIBs, so volume changes are accumulated during operation, meaning the initial optimal environment is not maintained in the long term. Additionally, the initial pressure cannot be optimized according to changes in the environment during operation because the initial compressive pressure is not changeable after manufacturing LIB modules and packs.

To overcome these limitations, this paper proposes a novel framework for active pressure management. To the best of our knowledge, no studies have been reported on the active pressure management of LIBs that can control both reversible and irreversible pressure changes during operation by deploying a simple and effective closed-loop control scheme in real time. Note that hydraulic or pneumatic actuation systems have been proposed to manage the pressure of LIB (Hahn et al., 2021; Deich et al., 2020). However, these systems are bulky and complex. Moreover, these systems require considerable space and energy consumption, suggesting that they are not feasible for applications of EVs. By contrast, the proposed method using a phase transition actuator is simple and economical to perform pressure management under limited space and weight conditions such as in EVs, implying that the proposed method would be the sole method for real-world applications. Specifically, the phase transition actuator with an equivalent mechanical stiffness is deployed to compensate for the volume changes in an LIB under constrained conditions. Furthermore, the dynamic characteristics of pressure variation for the phase transition actuator are characterized with respect to the accumulated current for elaborate active pressure management. Experiments on the proposed method demonstrated its effectiveness under a variety of stationary and stochastic operational conditions, suggesting that it is possible to maintain optimal pressure during real-world operations of LIBs. Therefore, the proposed method not only mitigates concerns regarding the accumulated stress caused by reversible pressure changes in each cycle, but also eliminates concerns regarding irreversible pressure changes during long-term operation. Remarkably, the accumulated stress of an LIB caused by pressure variation was reduced by 56.17% under stochastic operational conditions when activating the pressure management strategy, resulting in a 1.47% increase in discharge capacity immediately following operation compared to that under passive pressurized conditions. This result clearly demonstrates the effectiveness of the proposed method for real-world applications in EVs. The inherent simplicity and economic feasibility of the proposed method open the door for a new generation of battery management systems (BMSs) with active pressure management.

2. Experiments

Active pressure management was conducted with a 20 Ah pouch-type (width = 160 mm, height = 227 mm, and depth = 7.25 mm) lithium iron phosphate (LFP) cell as a target battery for pressure management. This LIB consists of stacked LFP cathodes, graphite anodes, and separators as its main components. The nominal potential is 3.3 V and the range of operational temperature is −30 to 55 °C according to the specification sheet. A phase transition actuator was implemented using a lithium nickel manganese cobalt oxide (NMC) battery. This phase transition actuator is a 26 Ah pouch-type (width = 161 mm, height = 227 mm, and depth = 7.5 mm) cell with a graphite anode, which has the greater capacity than the LIB of interest for effective pressure management. This battery was selected as a phase transition actuator because its equivalent stiffness is similar to that of the LIB of interest, suggesting that the equivalent stiffness of

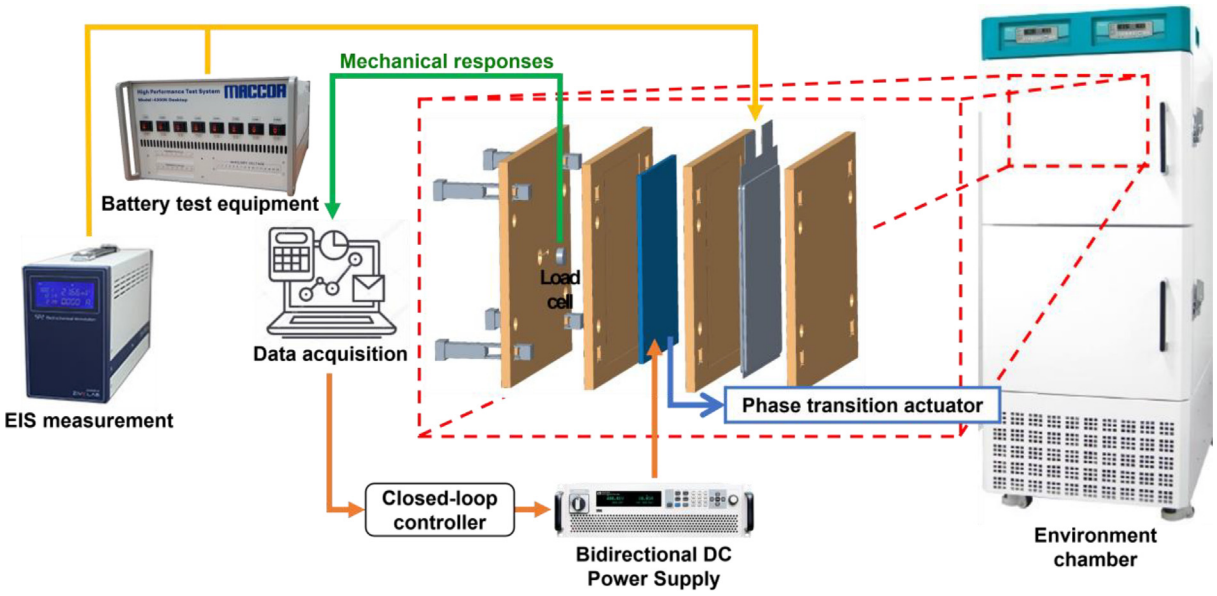

Fig. 1. Schematic diagram of the experimental setup.

an actuator plays an important role in active pressure management. It is worth noting that a piezoelectric actuator was used in a preliminary experiment for pressure control and management because such actuators are widely known for their large swelling characteristics relative to the imposed current (Tianze et al., 2009). However, a piezoelectric actuator cannot effectively control pressure under constrained conditions because the equivalent stiffness of a piezoelectric actuator is much less than that of a LFP cell (Kwak et al., 2020). It can be inferred that a small equivalent stiffness constrains the pressure management capabilities of this actuator under pressurized conditions, suggesting that the equivalent stiffness of the actuator is an important metric when selecting an appropriate actuator for the active pressure management of an LIB. This study aimed to manage the reversible swelling of an LIB caused by the phase transition of a graphite material (Ohzuku et al., 1993), implying that the reversible swelling of another battery can be used as an effective actuating force because the equivalent stiffness values of both batteries are similar. Among the many types of batteries with graphite anodes, an NMC battery was selected because the evolution of swelling under unconstrained conditions or that of compression pressure under constrained conditions is relatively linear compared to other batteries relative to the applied current (Oh et al., 2014). The detailed characteristics of this actuator are presented in Section 3. This paper uses the term "phase transition actuator" instead of "NMC battery" to avoid confusion with the LIB targeted for pressure management.

A schematic of the experimental setup is presented in Fig. 1. The test bench consists of two end plates, two middle plates, four rods, and fours stacks made of AL 6063. The two end plates are fixed by placing rectangular rods and stacks at the four corners of each plate and the initial pressure is determined by the thickness of the stacks (Kim et al., 2021). This configuration is more effective for ensuring repeatability in long-term experiments compared to using compression pressure induced by bolts and nuts, which makes it difficult to guarantee the same initial compression pressure after several charge/discharge cycles as a result of loosening effects (Kim et al., 2021). A load cell (Omega LCKD-1000, USA) with a capacity of 4448 N and repeatability of 0.10% in terms of full-scale output is installed on the end plate to measure the pressure induced by reversible swelling during phase transition. This measurement is also used to calculate feedback signals by identifying the current state of a cell during active pressure management. The two middle plates uniformly transmit the pressure caused by swelling and deformation in the LIB and phase transition actuator because the equivalent stiffness of plates is much greater than that of the LIB and phase transition actuator (Kwak et al., 2020). This relatively high stiffness of the middle plates compared to the cells also ensures a homogeneous pressure distribution during pressure measurement and management.

To evaluate the feasibility of the proposed control strategy and pressure management scheme, active pressure management was conducted under a variety of operational conditions, as shown in Table 1. All experiments were conducted at constant temperature of 25 °C in an environmental chamber (Jeiotech LCH-11-2C, Korea). The LIB under pressure management was charged and discharged using battery testing equipment (MACCOR 4300K, USA), whereas the feedback current was independently applied to the phase transition actuator through a bidirectional DC power supply (ITECH IT6000C, Taiwan). Each experiment began by setting the accumulated current of the phase transition actuator to 15 Ah, which corresponds to 57.7% of the state of charge (SOC) of the phase transition actuator. This setting can be explained by the fact that the total actuating pressure range covers 17.15 kPa from 76.37 to 59.22 kPa, meaning the middle of the actuating pressure range is 69.76 kPa, which corresponds to 57.7% of the SOC of the phase transition actuator as a result of nonlinear pressure evolution with respect to the applied current. In other words, the widest region of pressure management was achieved by beginning in the middle of the excitation pressure range of the phase transition actuator. Then, the pressure was controlled in real time using an active control scheme when the targeted LIB was operated under predefined operational conditions.

In the first experimental set (Case # 1 in Table 1), the hypothesis that the lifespan of an LIB could be managed using an active control scheme was validated by measuring the equivalent impedance and capacity of the target LIB under different pressurized conditions. Specifically, this experiment would reveal that the equivalent impedance of the LIB changed under different pressurized conditions because its overpotential depends on the constraint conditions (Barai et al., 2013; Williard et al., 2021). Furthermore, this experiment aimed to confirm the dependency of the measured capacity on pressurized conditions, which is an

Table 1
Pressure management experimental conditions.

Case #	Objective	Current profile [C]	Setpoint pressure [kPa]	Temperature [°C]
1	Hypothesis validation	0.5	69.76[a] 69.76	25
2	Trajectory tracking w/constant setpoint	0.5	69.76[a] 69.76–74.30 (= SOC 0%–100% w/10% interval)	25
3	Step pressure tracking	0.5	69.76[a] Step function (up-down) Step function (down-up)	25
4	Rate dependency	1.0 2.0	69.76[a] 69.76 (= SOC 0%)	25
5	Driving cycle	US06	73.28[a] 73.28 (= SOC 50%)	25

[a]w/o control.

indirect, but general indicator of an LIB lifespan. Therefore, the correlations among pressure, equivalent impedance, and capacity were clearly determined by comparing experiments with and without the active pressure management strategy. Specifically, the pressure value of 69.76 kPa was defined as the setpoint and active pressure management was conducted using the phase transition actuator. The LIB of interest was fully charged using the constant current-constant voltage (CCCV) protocol up to 3.5 V and then fully discharged using a protocol of constant current (CC) down to 2.0 V at a fixed C-rate of 0.5 C. Finally, 2 h of relaxation were allowed after fully charging and discharging the LIB. The capacity of the LIB was calculated using a Coulomb counting method. Additionally, electrochemical impedance spectroscopy (EIS) was performed using a single-channel electrochemical workstation (WonATech ZIVE LAB SP2, Korea) when the pressure reached predefined setpoints during discharge at predefined SOCs of 100%, 75%, 50%, 25%, and 0%. Specifically, the LIB of interest was fully charged with the CCCV protocol up to 3.5 V at a fixed C-rate of 0.5 C, discharged with the CC protocol to 25% of its initial capacity at a fixed C-rate of 0.1 C, and then subjected to EIS. Discharge and EIS were repeated until the LIB was fully discharged with 2 h of relaxation after reaching the fully charged and discharged states.

The second experimental set aimed to evaluate the pressure management capabilities of the proposed method under stationary operational conditions. Three types of experiments were conducted when the LIB of interest was charged and discharged following the same protocol used in the first experimental set. First, the performance of trajectory tracking was evaluated with different setpoints for the pressure (Case #2 in Table 1). Specifically, 11 pressure values from 0 to 100% of the SOC with 10% SOC intervals were defined as setpoints in an active control scheme while the LIB of interest was operated under a stationary discharge condition at a C-rate of 0.5. Second, the upward and downward step profiles of compression pressure were tracked using the active control scheme (Case #3 in Table 1) with the goal of analyzing control performance under significant loading conditions because the optimal LIB pressure can vary significantly during operation (Mussa et al., 2018). The upward and downward step profiles comprised six intervals that evenly divided a pressure range of 0 to 100% of the SOC of the LIB. Therefore, the compression pressure was managed using this predefined profile for the phase transition actuator when the LIB was fully charged and discharged. Third, pressure management performance was analyzed under rapid charge and discharge conditions because LIBs often suffer from rapid charge and discharge in real-world applications (Case# 4 in Table 1). Specifically, the pressure corresponding to 0% of the SOC of the LIB was defined as a setpoint and the LIB of interest was charged and discharged at C-rates of 1.0 C and 2.0 C.

In the third experimental set (Case #5 in Table 1), active pressure management was conducted under stochastic operational conditions to demonstrate the capabilities of the proposed pressure management scheme for EV applications. Specifically, active pressure management was conducted with pressure values corresponding to 25%, 50%, and 75% of the SOC of the LIB while the LIB underwent charge and discharge with the current profile of the US06 driving cycle, which is a high-driving-load condition defined in the United States (US Environmental Protection Agency, 2006). An initial pressure corresponding to 50% of the SOC of the LIB was defined as a setpoint because the initial SOC was 50%. This SOC is the most frequently used in EVs (Scrosati and Garche, 2010).

3. Active pressure management strategy

A schematic of a normal constrained operation with a fixed constant pressure is presented in Fig. 2(a), whereas a schematic of an operation with active pressure management through a phase transition actuator is presented in Fig. 2(b). Specifically, the LIB of interest is in a fully delithiated state, where it is constrained and subjected to constant initial pressure in an LIB module and pack (Fig. 2(a-i)). In this scenario, the distance between the two end plates decreases under the initial pressure, resulting in the initial deformation δ_i of the LIB. Therefore, the initial pressure $P_{initial}$ is generated as $|k_B\delta_i/Area|$ by the imposed constrained condition. It is assumed that this initial pressure is optimal for minimizing the equivalent impedance of the LIB, thereby maximizing the lifespan of the LIB. However, the LIB will suffer from pressure variation during operation as a result of the phase transition of graphite anode materials (Fig. 2(a-ii)). Specifically, the LIB becomes partially or fully lithiated, where the transportation and diffusion of lithium ions changes the molecular structure of the cathode and anode materials, resulting in a macroscopic volume change δ_s of the LIB (Siegel et al., 2013; Lee et al., 2003). This phenomenon is defined as free swelling in the direction perpendicular to the electrodes under unconstrained conditions. However, the free swelling δ_s transforms into compression pressure $P_{swelling}$ under constrained conditions, implying that the pressure imposed to the LIB varies with the SOC during operation because phase transition depends on the SOC. This pressure variation during charge and discharge accumulates internal stress in the positive and negative electrodes, increases micro cracking, thickens SEI layers, and decreases the lifespan of LIBs.

In the active scheme for pressure management, the LIB of interest is in a fully delithiated state and assembled to the actuator in series with a certain amount of charge states (Fig. 2(b-i)).

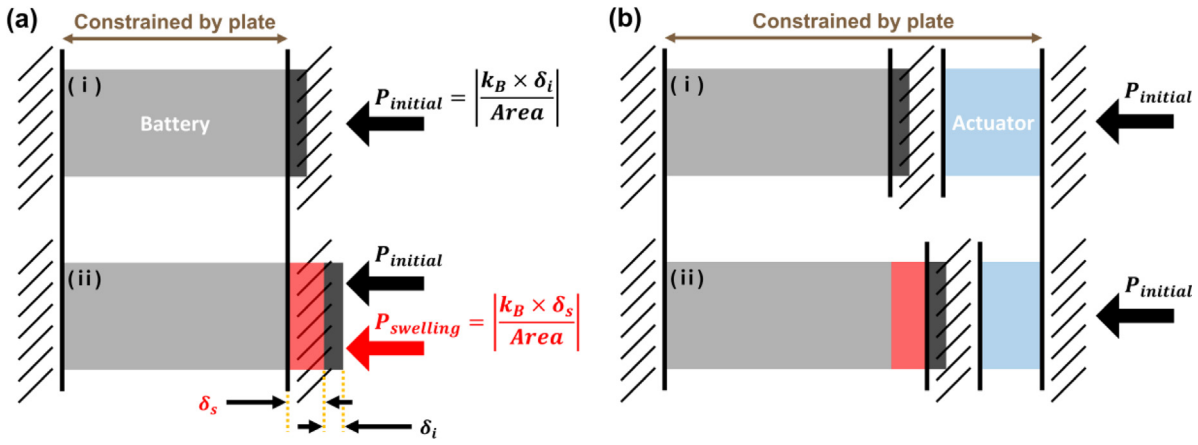

Fig. 2. Constraint conditions for an LIB with initial pressure $P_{initial}$ (a-i) in the passive and (b-i) active control schemes, and SOC changes during operation (a-ii) in the passive and (b-ii) active control schemes.

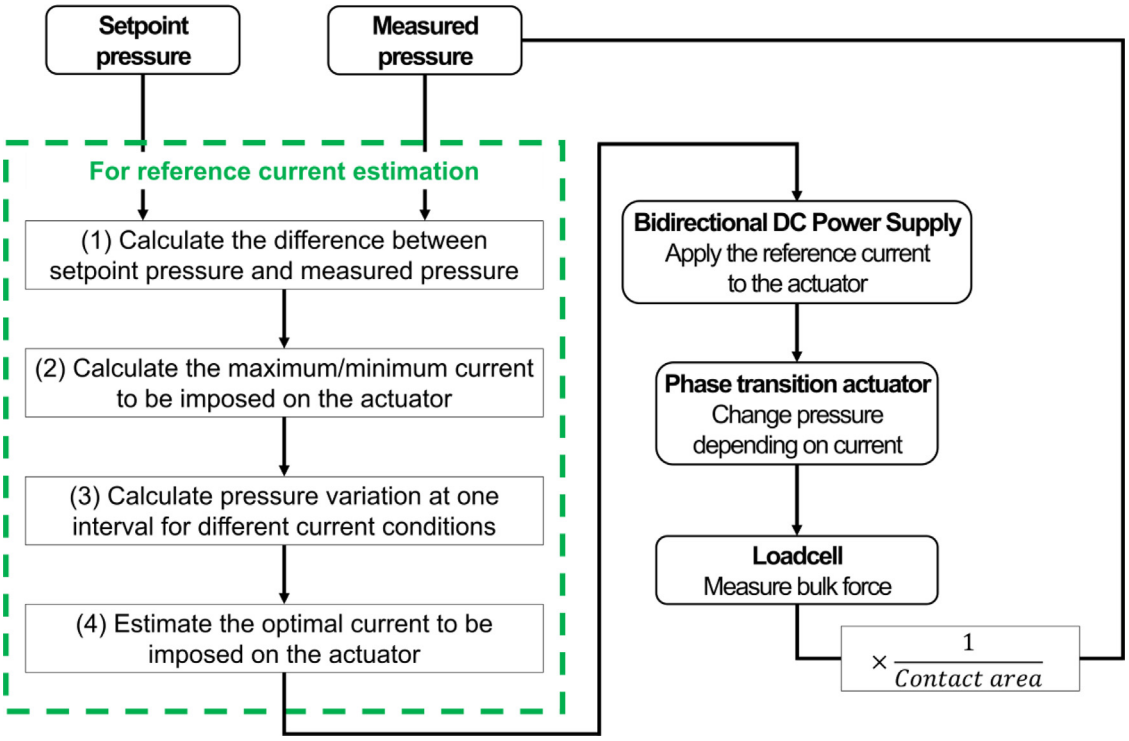

Fig. 3. Flowchart of the proposed control method for pressure management.

The entire system is also subjected to a constant optimal initial pressure. Therefore, the same $P_{initial}$ (i.e., $|k_B\delta_i/Area|$) is being applied to the LIB because the initial deformation is the same as the initial displacement δ_i (Fig. 2(a-i)). Then, the charge state of the LIB changes to a partially or fully lithiated state during operation in the active pressure management scheme (Fig. 2(b-ii)). The LIB is charged, resulting in the free swelling δ_s, but the actuator is delithiated to the opposite degree of swelling $-\delta_s$ in the LIB of interest, meaning the free swelling δ_s of the LIB is canceled by the free swelling $-\delta_s$ of the actuator, resulting in no change in the pressure imposed on the LIB, even though the LIB experiences swelling-induced pressure under typical operational conditions. As a result, the LIB can always be subjected to an optimal pressure state during operation.

A simple closed-loop control method was introduced for effective pressure management with a sampling frequency of 0.5 Hz (Fig. 3). Specifically, four phases are iterated in a control loop to estimate the current imposed on the phase transition actuator. First, the difference between the setpoint pressure and pressure measured by a load cell is calculated at time t. The measured bulk force is transformed into pressure by dividing the measured bulk force by the equivalent contact area of the LIB. Second, the maximum/minimum current that can be imposed on the LIB of interest is determined based on the accumulated current in the actuator at time t. The phase transition actuator is an LIB of the NMC type, meaning the maximum/minimum current is limited by the accumulated current of the actuator as a result of the overpotential phenomenon. Note that this paper uses the term of "accumulated current" for the phase transition actuator instead of SOC to avoid confusion between the SOC of the LIB of interest and that of the phase transition actuator. Third, the pressure variation in one interval (2 s) of the actuator is calculated

Table 2
Current limit of the phase transition actuator with respect to the accumulated current.

Accumulated current (Ah)	0–20.7	20.7–23.1	23.1–24.6	24.6–25.3	25.3–26	26.0–26.5	26.5–27.0	27.0–
Maximum/minimum current (A)	±52	±39	±26	±19.5	±13	±7.8	±2.6	±1.3

for 1001 different current conditions. Specifically, this estimation is performed for a current range of 0 to 52 A in intervals of 0.052 A to secure high accuracy for the proposed active pressure management scheme. Fourth, the pressure differences between the pressure to be offset and pressure variation estimated in the current range of interest are calculated to determine the optimal current that minimizes these differences and is between the maximum and minimum current determined in the second phase. These four phases are iterated to generate a reference signal in the proposed control method. It is worth noting that this simple closed-loop control method is sufficient for the proposed method because the diffusion dynamics of an LIB are slow. Future work includes a complex and robust control method for improving active pressure management.

This control strategy can manage both reversible pressure caused by phase transition during short-term operation and irreversible pressure evolution caused by SEI formation during long-term operation because the proposed control strategy only considers differences between the setpoint and measurements, ensuring that the proposed method will be effective in various scenarios. Identifying the characteristics of the phase transition actuator is important for estimating the optimal current to be applied to the actuator to secure control performance in real-time applications.

A phase transition actuator with a capacity greater than that of the target LIB should be used for effective pressure management. The phase transition actuator has nonlinear characteristics of stress and volume deformation with respect to its accumulated current (i.e., SOC) when a current is applied as a result of the nonlinear phase transition of its graphite anode (Oh et al., 2016). Therefore, the dynamic characteristics of the phase transition actuator were identified first to construct a lookup table, which is used in the third phase to calculate pressure variation in the proposed method for effective pressure control with a variety of constant currents, including 1.3, 2.6, 7.8, 13, 26, 39, and 52 A (Fig. 4(a)). These currents correspond to C-rates of 0.05, 0.1, 0.3, 0.5, 1.0, 1.5, and 2.0 C with consideration for the total accumulated current in the actuator. The maximum accumulated current depends on the C-rate of the current applied based on overpotential (Fig. 4(a)) (Oh et al., 2014). The smaller the C-rate, the more significant the nonlinear behavior that occurs in both the charge and discharge curves because a single phase is dominant under low-C-rate operational conditions. In contrast, multiple phases coexist in the phase transition actuator at a high C-rate (Kwak et al., 2020), resulting in a moderate nonlinear phenomenon in the swelling-induced pressure with respect to the accumulated current. Hysteresis between charge and discharge curves also exists in mechanical responses (Fig. 4(b) and (c)), which originates from lithium-ion concentration during charge and discharge (Ovejas and Cuadras, 2019), suggesting that the dynamic characteristics of the phase transition actuator are highly nonlinear in different operational ranges. The dotted lines in Fig. 4(b) and (c) represent the maximum accumulated current corresponding to the C-rate. However, a safety margin of 0.28 Ah was defined based on the maximum accumulated current in a feedback control loop to mitigate concerns regarding side reactions caused by overcharge. Detailed values are listed in Table 2. This analysis yields the relationship between the pressure and accumulated current in the phase transition actuator, resulting in a lookup table for the phase transition actuator for charge and discharge states (Fig. 4(d) and (e)).

4. Results and discussion

4.1. Validation of the hypothesis

To verify the hypothesis that the lifespan of an LIB is manageable through the proposed pressure management strategy, the effects of active pressure management on the dynamic characteristics of an LIB are analyzed. This study indirectly analyzed the correlation between compressive pressure and the dynamic characteristics of an LIB because a degradation experiment using the proposed method would require a long period of time. Future work includes the direct validation of the proposed active pressure management method through a long-term degradation experiment.

The pressure evolution measured with and without the active pressure management strategy is presented in Fig. 5(a). Specifically, the blue and red lines represent pressure evolution with and without the proposed active control scheme, respectively. The setpoint for the pressure was 69.76 kPa during operation when activating the pressure management strategy. To compare the effects of active pressure management on LIB performance and characteristics, the potential under a charge condition and equivalent impedance under a discharge condition are also compared in Fig. 5(b) and (c).

Remarkably, the proposed active control strategy follows the setpoints accurately, as shown in Fig. 5(a), suggesting that the proposed active control scheme effectively manages the pressure imposed on the LIB of interest. Detailed analysis on the capabilities of the proposed control strategy is presented in the following subsection.

The potential curves with and without the active pressure management exhibit different dynamic responses for the LIB (Fig. 5(b)). Note that experiments were conducted three times for each case to confirm the repeatability of the dynamic response by pressure management and the potential was averaged. The standard deviation of the potential measured with and without pressure management was 0.0025 V and 0.0050 V, verifying the phenomenon of the same trend in experiments. Note also that the standard deviation for each case is not shown in Fig. 5(b) because it is too small to be illustrated in Figure. The potential increases rapidly in the CC charge mode and quickly reaches the limit value of the CC mode, switching to a CV mode when charging the LIB without active pressure management (Fig. 5(b)). It can be inferred that a decrease in the equivalent overpotential results in this difference in the charge curve because appropriate pressure would decrease the equivalent impedance of the LIB (Dsoke et al., 2013). The difference in equivalent surface impedance also results in different capacities for charge and discharge. Specifically, the charge and discharge capacities are 20.120 and 20.018 Ah with active pressure management, whereas they are 20.015 and 20.015 Ah under the passive constrained condition, suggesting that the charge and discharge capacities increases by 0.525% and 0.015% when activating the pressure management strategy. This difference is small, yet distinct because improvements in LIB impedance caused by active pressure management are accumulated over the entire lifespan of an LIB. The total increase would be 15% based on the discharge increment if degradation is linear and the total lifespan is 1000 cycles. However, degradation is nonlinear because several factors including loss of lithium inventory, loss of active material, and conductivity loss, affect the lifespan of LIBs (Pastor-Fernández et al., 2017), suggesting that further

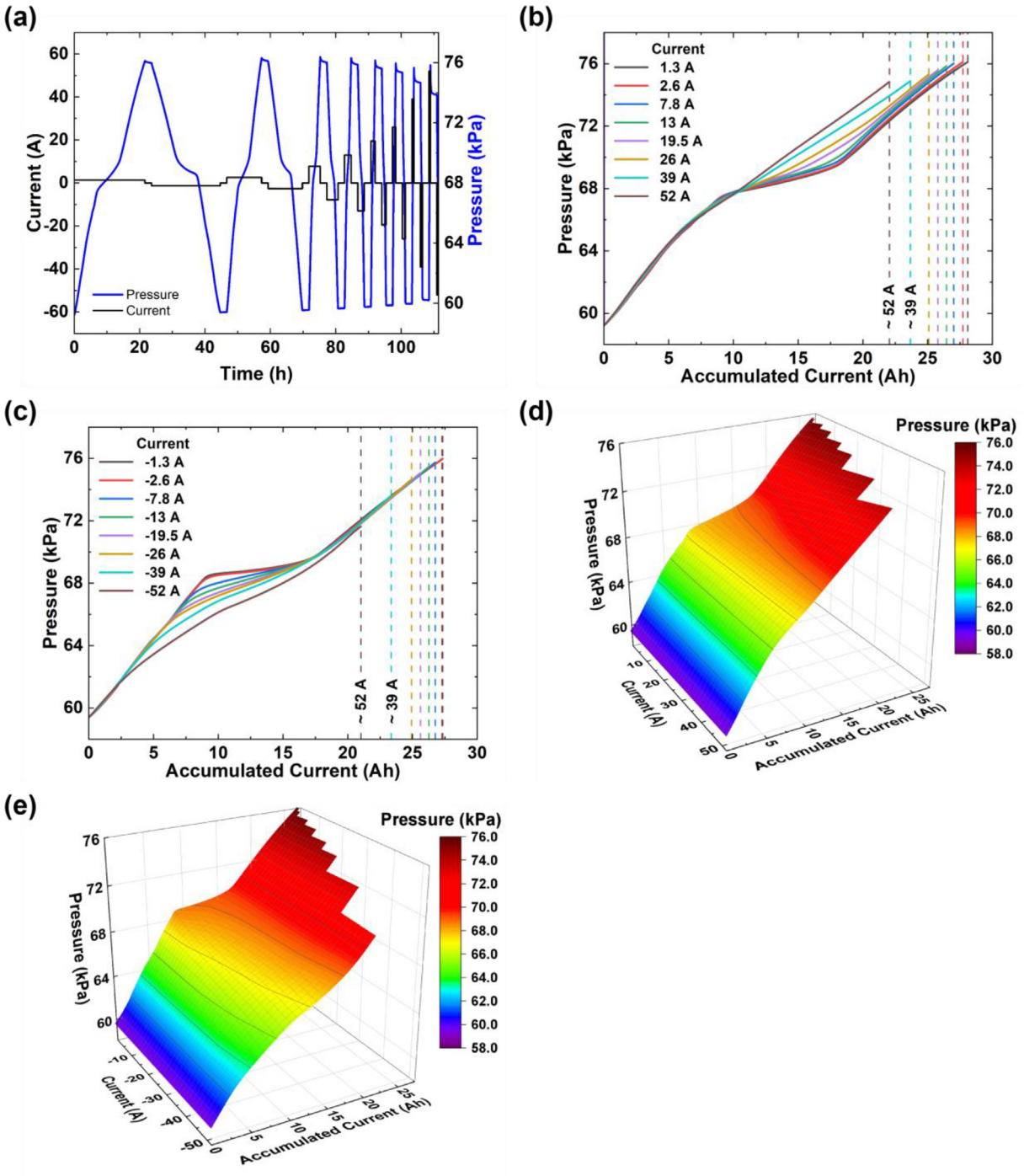

Fig. 4. Evolution of (a) current and pressure (indicated by black and blue, respectively) during dynamic characterization. Dynamic response during (b) charge and (c) discharge according to current. Lookup table constructed by interpolating and extrapolating the dynamic responses of the phase transition actuator during (d) charge and (e) discharge. (For interpretation of the references to color in this figure legend, the reader is referred to the web version of this article.)

studies should be conducted to elucidate quantitative lifespan enhancement when employing an active pressure management strategy for LIBs.

The role of active pressure management is clearly highlighted in the EIS results. Specifically, the frequency range of 0.1 to 1 Hz in the EIS results (blue shaded region in Fig. 5(c)) is shifted from the right to the left in the EIS spectrum measured at the SOC of 50% when activating pressure management, suggesting that the equivalent impedance in this frequency range decreases with active pressure management. This observation also suggests that active pressure management affects the diffusion of LIBs because this frequency is highly correlated with diffusion phenomena during charge and discharge (Kim and Monroe, 2013). Specifically, the constant pressured measured implies that the porosity is constant in an optimal state with active pressure management during operation, whereas porosity changes depending on operational conditions in a passive pressure scheme. Therefore, porosity variation adversely affects the diffusion of lithium ions under passive pressurized conditions. The real-axis intersection of the EIS spectrum also shifts to the left in the measured equivalent impedance when activating pressure management (circled inset in Fig. 5(c)). This intersection represents the equivalent resistance

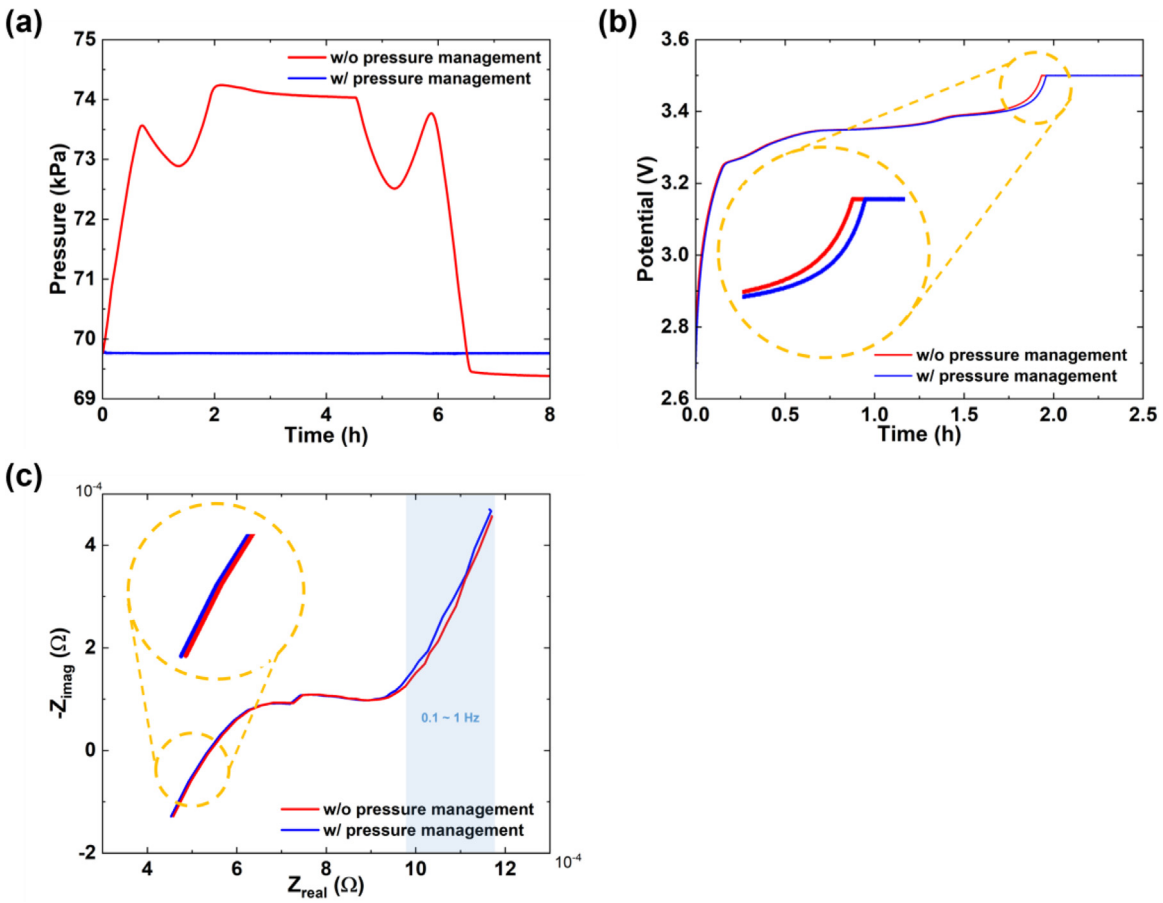

Fig. 5. (a) Evolution of pressure without pressure management (red) and with pressure management (blue). Comparison of (b) potential and (c) impedance without pressure management and with pressure management. (For interpretation of the references to color in this figure legend, the reader is referred to the web version of this article.)

in the boundaries between SEI layers, charge transfer region, and ohmic region (Sihvo et al., 2020), suggesting that high-frequency harmonics from active pressure management contribute to the equivalent resistance at this frequency. In other words, the equivalent overpotential decreases proportionally to the reduction in equivalent impedance, meaning the entire EIS curve shifts from right to left when activating the active pressure management strategy. The same trends can also be observed in the impedance measured at other SOCs, but are not shown here for the sake of brevity. High equivalent impedance in an LIB increases the accumulated stress in the microstructures of anode materials under passive pressure constrained conditions because periodic stress causes cracks to form SEI layers on the surface of the anode, as well as the destruction of particles. Therefore, accumulated stress accelerates the fatigue failure of active materials (Peabody and Arnold, 2011).

In conclusion, the equivalent impedance of an LIB depending on compression pressure affects the equivalent overpotential during operation, meaning it affects the capacity and lifespan of the LIB. Excessive pressure accelerates aging, whereas optimal pressure improves contact efficiency and reduces the occurrence of lithium plating (Fang et al., 2021; Shen et al., 2021; Zhang et al., 2019), suggesting that the lifespan of LIBs depends on the initial pressure under passive constrained conditions. Reversible pressure variations inevitably occur in an LIB under passive constrained conditions because the phase transition of active materials occurs during operation. Irreversible pressure changes also increase as the LIB ages based on the growth and formation of SEI layers, further accelerating degradation phenomena. In contrast, the proposed active pressure management strategy can operate the LIB in an optimal environment by maintaining a constant porosity because active pressure management compensates for the swelling of LIBs originating from phase transitions. The proposed method can also mitigate concerns regarding the stress accumulation caused by irreversible pressure increases during operation. However, further analysis of degradation and aging phenomena would be helpful for establishing an elaborate active pressure management strategy for controlling irreversible pressure, suggesting that a future study should include systematic identification of the origins of degradation mechanisms in LIBs.

4.2. Pressure management under stationary operational conditions

Experiments on trajectory tracking are presented in this subsection to demonstrate the capabilities of active pressure management with different setpoints. Specifically, 11 experiments were conducted with 11 different setpoints from 0% to 100% of the SOC in 10% intervals. Fig. 6(a) presents the control capabilities for four setpoints of 69.76, 71.11, 72.31, and 74.16 kPa, corresponding to 0%, 10%, 20%, and 100% of the SOC of the LIB. Comparisons to the pressure evolution under passive pressure conditions (red line in Fig. 6(a)) reveal that the active control strategy follows all set pressure values accurately. Specifically, the root-mean-squared errors (RMSEs) are 0.0027, 0.0551, 0.1393, and 0.2209 kPa after reaching the settling time for each setpoint, respectively. The settling time is defined as the time required to settle within 5% of the setpoint. In the transient response (gray-dashed inset in Fig. 6(a)), it can also be observed that

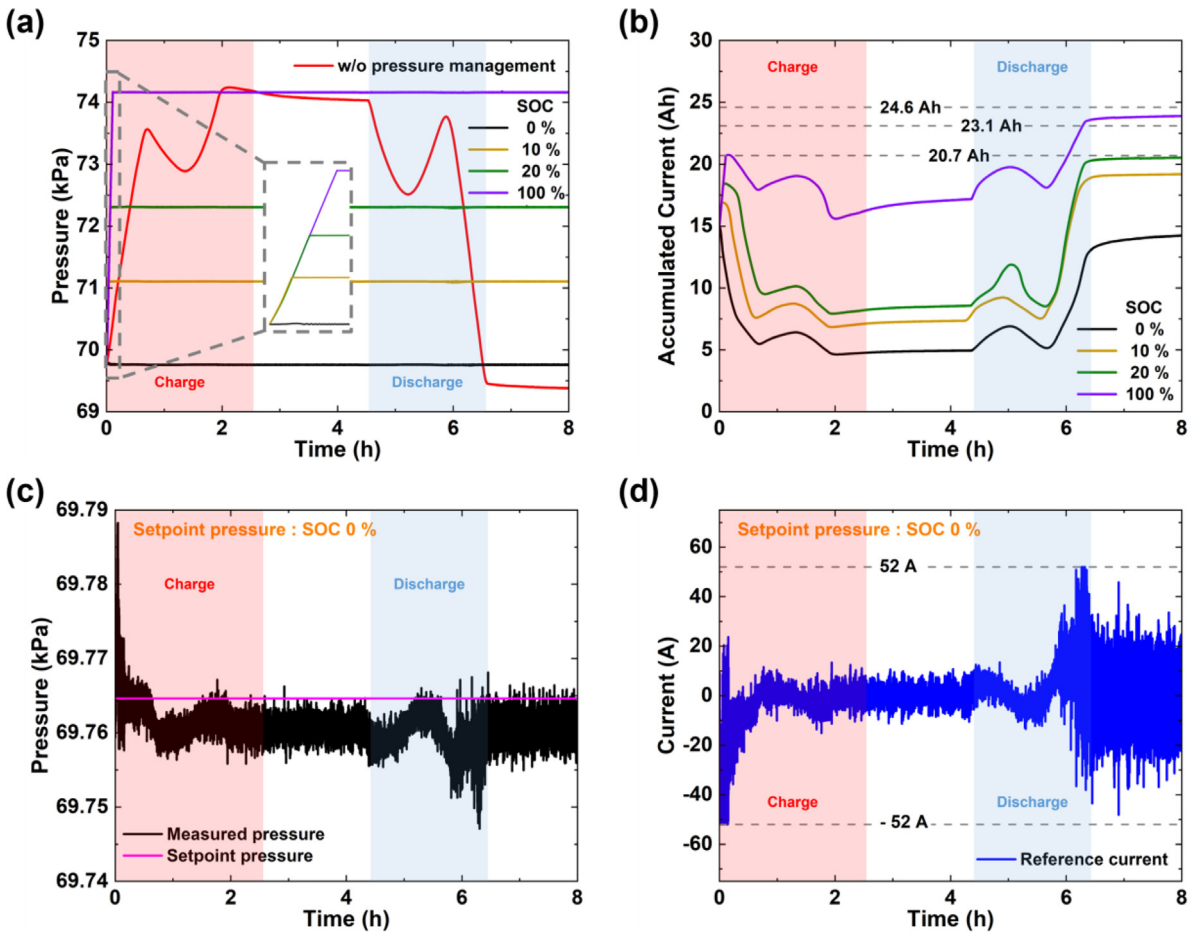

Fig. 6. Trajectory tracking experiment: (a) pressure, (b) accumulated current in the phase transition actuator, (c) pressure at 0% of the SOC control, (d) calculated current (blue) applied to the actuator at 0% of the SOC control. (For interpretation of the references to color in this figure legend, the reader is referred to the web version of this article.)

the rise times for each setpoint corresponding to 10%, 20%, and 100% of the SOC of the LIB are 102, 180, and 304 s, respectively. For the setpoint corresponding to 0% of the SOC, the initial pressure is the same as the setpoint. These results suggest that the proposed control strategy successfully reaches the setpoint within a short period (approximately six minutes). Therefore, the proposed method can be deployed in a BMS requiring a short time constant and high control accuracy. Note that total variation from 0% to 100% of the SOC within six minutes would be a short time considering the slow diffusion phenomenon of LIBs and a phase transition actuator. It is also worth noting that the proposed method is economical because phase transition actuators (i.e., NMC type of battery) are cheap.

To control the compressive pressure based on setpoints, a current was applied to the phase transition actuator with an initial accumulated current of 15 Ah (excluding the setpoint corresponding to 0% of the SOC) during the transient period. The phase transition actuator was then discharged to maintain a constant setpoint pressure during a charge period (transparent red region in Fig. 6(b)), reaching values of 4.73, 7.02, 8.15, and 16.05 Ah corresponding to each setpoint. The accumulated current increased again during a discharge period (transparent blue region in Fig. 6(b)) because the phase transition actuator was charged to compensate for the volume change in the LIB of interest. Small variations in accumulated current in charge and discharge regions originate from the compensation of phase transition regions of the LIB because the SOC of the LIB corresponds to nonlinear phase transition regions, suggesting that pressure variation caused by phase transitions in the LIB are also successively compensated by the proposed method. The accumulated current is kept lower than 20.7 Ah during trajectory tracking (excluding the setpoint corresponding to 100% of the SOC), suggesting that the usable current range of the actuator is approximately −52 to 52 A. This wide range of applicable current is one reason for the accurate pressure management capabilities of the proposed method.

Detailed analysis of the active pressure management experiment for the setpoint corresponding to 0% of the SOC is presented in Fig. 6(c) and (d). The maximum variation between the setpoint (pink line) and measurements (black line) is 0.02 kPa (Fig. 6(c)), suggesting that the proposed method accurately manages pressure during operation. The difference between the maximum and minimum measured pressure is 0.04 kPa, confirming that the proposed control strategy ensures high accuracy. This observation can be explained by the fact that characterization of the phase transition actuator is accurate, meaning the proposed control strategy elaborately estimates the optimal current to be imposed on the phase transition actuator (Fig. 6(d)). Specifically, most of the current applied to the phase transition actuator is smaller than the maximum applied current range of −52 to 52 A (gray-dotted line in Fig. 6(d)), confirming that the compression pressure of the LIB varies in a controllable region in every interval.

To secure the control capabilities of the proposed method, additional experiments were conducted with step charge and discharge pressure profiles with six intervals when charging and

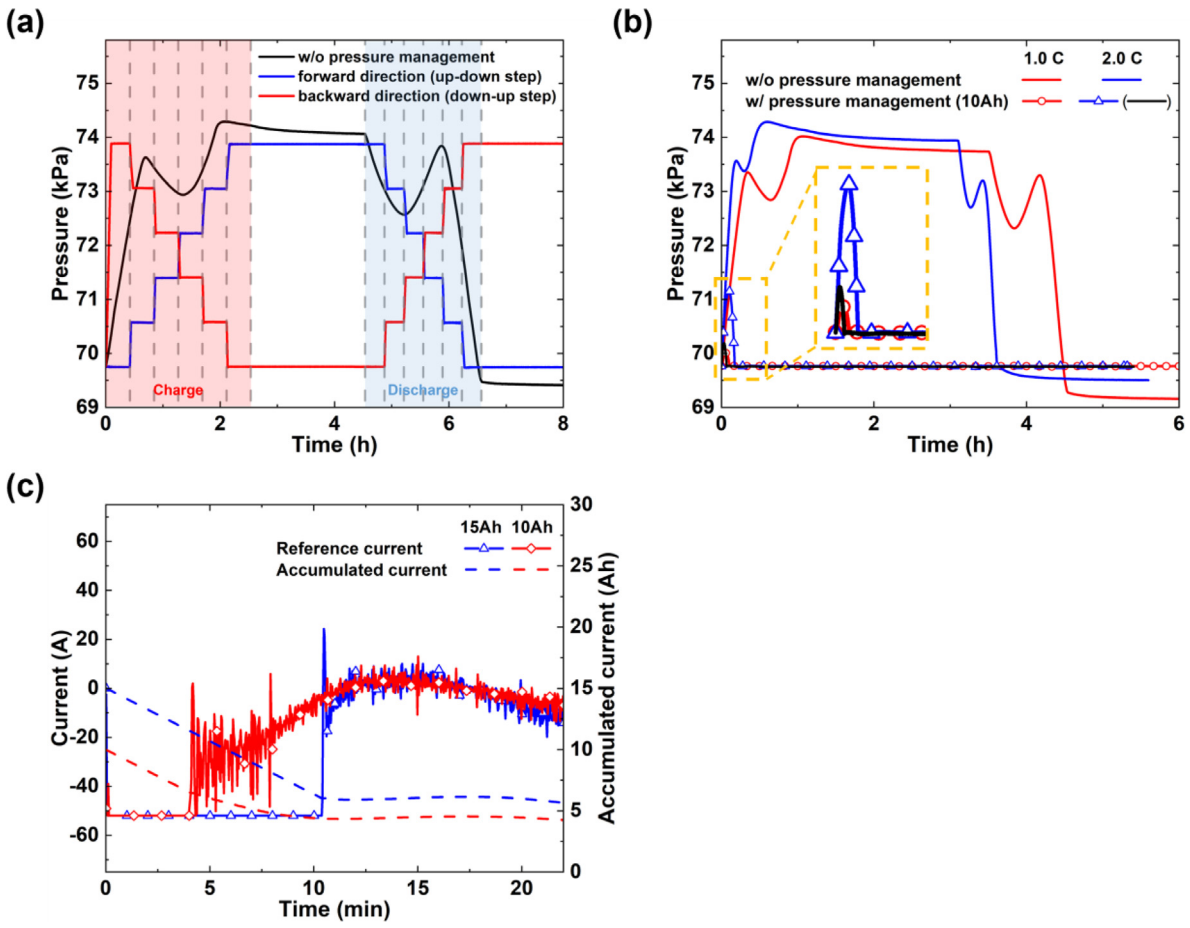

Fig. 7. Evolution of pressure in the (a) step pressure experiment and (b) rate dependency experiment. (c) Evolution of the reference current and accumulated current of the initial response (yellow inset figure).. (For interpretation of the references to color in this figure legend, the reader is referred to the web version of this article.)

discharging the LIB at a fixed C-rate of 0.5 C. These experiments also replicated a scenario in which the optimal pressure changes depending on environmental conditions, meaning the setpoint for the optimal pressure could change during operation. In Fig. 7(a), the blue line represents the evolution of compression pressure with the reference input in the forward direction of LIB pressure change (six steps of compression pressure increase during charging and six steps of compression pressure decrease during discharging), whereas the red line represents the evolution of compression pressure with the reference input in the backward direction of LIB pressure change (six steps of compression pressure decrease during charging and six steps of compression pressure increase during discharging). One can see that pressure management in the backward direction is harsher than that in the forward direction because the amount of actuating pressure is greater than that in the forward direction. Remarkably, the proposed method accurately manages the compression pressure by following the predefined pressure profile in both directions. Specifically, the maximum rise time is less than three minutes in both directions, suggesting that the proposed method is sufficient for controlling pressure evolution caused by the phase transition of active materials in the LIB of interest in each cycle.

The proposed active pressure management strategy was also analyzed at different C-rates of 1.0 and 2.0 C because an LIB is often charged and discharged at various C-rates in the operation of EVs (Fig. 7(b)). This experiment also aimed to check whether the proposed method works at a high C-rate because the pressure variation in each interval required from the phase transition actuator will increase in proportion to the pressure variation of the LIB, which increases at a high C-rate. The overall management performance is good, except for in the initial stages. Specifically, the total pressure variation without and with pressure management decreases by 94.47% from 4.87 to 0.27 kPa at a C-rate of 1.0 C and by 70.29% from 4.78 to 1.42 kPa at a C-rate of 2.0 C. These phenomena can be explained by the fact that the pressure required exceeds the limit of the phase transition actuator as a result of moderate pressure variation in the phase transition actuator at the corresponding accumulated current. Specifically, the reference pressure required to compensate for the pressure variation of the LIB is 14.7 Pa in this region. However, the actual pressure change supplied by the actuator is only −11.1 Pa as a result of moderate variation in the slope of pressure for the actuator. Therefore, the difference between the reference and actual pressure increases as a result of this phenomenon. This phenomenon occurs because the phase transition actuator has nonlinearity, even though an NMC-type of LIB has relatively weak nonlinearity of pressure variation with respect to the corresponding accumulated current.

A steeper slope of pressure variation would be effective for mitigating this phenomenon during active pressure management. The initial accumulated current in the actuator was changed to 10 Ah to validate this hypothesis because the pressure variation in this region is greater than that at the accumulated current of 15 Ah. This experiment was only conducted by charging and

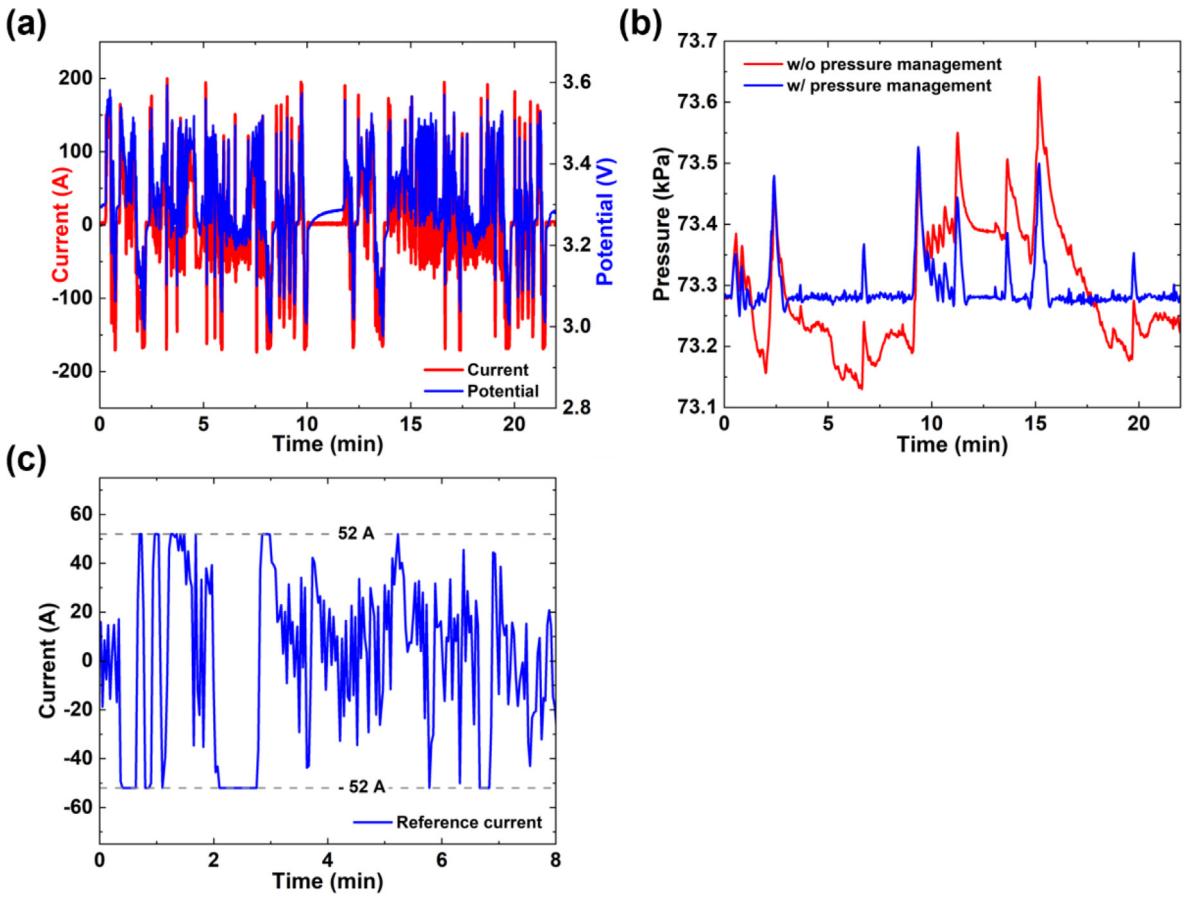

Fig. 8. (a) Current (red) and potential (blue) profile applied to the LIB. (b) Pressure evolution with (blue) and without (red) pressure management. (c) Current applied to the phase transition actuator calculated for pressure management.. (For interpretation of the references to color in this figure legend, the reader is referred to the web version of this article.)

discharging the LIB at a C-rate of 2.0 C. The experimental results are represented by the black line at Fig. 7(b). The total pressure variation is 0.43 kPa at the accumulated current of 10 Ah, whereas that was 1.42 kPa at the accumulated current of 15 Ah, suggesting that the maximum error is three times smaller compared to the previous result. This analysis clearly suggests that accumulated current in the phase transition actuator also plays a critical role in active pressure management considering the nonlinear pressure variation of the phase transition actuator with respect to the current imposed and accumulated current. The calculated reference current for the actuator (Fig. 7(c)) more clearly highlights these phenomena. During initial operation, the original saturation current of −52 A was applied because the pressure variation of the LIB was significant. However, the required reference current decreases faster at the initial accumulated current of 10 Ah compared to the initial accumulated current of 15 Ah because pressure variation (i.e., gradient of pressure with respect to the current applied) is more significant at the initial accumulated current of 10 Ah. It should be noted that the total manageable pressure region and error for pressure management have a trade-off relationship. The initial accumulated current of 15 Ah has a wide bidirectional range of pressure management, but slow pressure response at initial, whereas that of 10 Ah ensures rapid compensation for pressure variation, but has a smaller pressure range for discharge, suggesting that engineers should tune this parameter for applications of the proposed method to various applications.

4.3. Pressure management under stochastic operational conditions

To demonstrate the applicability of the proposed method for real-world applications, active pressure management was deployed in an experiment of the US06 driving cycle (Fig. 8(a)). The US06 driving cycle is a representative stochastic high load driving condition for EVs in the United States (US Environmental Protection Agency, 2006). The current imposed on the battery pack of a Ford Fusion hybrid vehicle was considered in this study based on Ref. Oh and Epureanu (2017). Specifically, the current imposed on a single cell was calculated and then the corresponding C-rate was estimated based on the capacity of a single cell from Ref. Oh and Epureanu (2017). Then, the current applied to the LIB of interest was estimated based on the C-rate and capacity of the LIB of interest. Finally, the estimated current profile was imposed on the LIB (red line in Fig. 8(a)) and the potential was also measured (blue line in Fig. 8(a)). The measured pressure with (blue line) and without (red line) active pressure control is presented in Fig. 8(b). The current imposed on the phase transition actuator is also presented in Fig. 8(c). This experiment was conducted with an initial SOC of 50% for the LIB of interest. Note that safety implications should be considered for real-world applications because ohmic heat occurs in both the targeted LIB and phase transition actuator. However, a safety issue was not considered during this experiment because the surface temperature measured at the center of the targeted LIB only increased by up to 3 °C even though the US06 driving cycle is a representative stochastic high load driving condition. It might be originated from

a good cooling condition of the environmental chamber used. A study on effective thermal management strategies of the LIBs would be effective to embed the proposed method for real-world applications, which are also important research topics of LIBs actively studied (Wu et al., 2019; Kim et al., 2019; Wang and Ma, 2017).

Remarkably, the pressure variation is significantly reduced when the active pressure management strategy is deployed, suggesting that the proposed active pressure management strategy decreases the compressive pressure imposed on LIBs even under the stochastic operational conditions of EVs. Specifically, the RMSE with and without the active pressure management strategy is 0.0455 and 0.1038 kPa, respectively, suggesting that the stress accumulated in the LIB is reduced by 56.17%. This reduction is significant when considering the total lifespan of the LIB. Additionally, the remaining discharge capacity with and without pressure control is 9.961 and 9.816 Ah immediately after completing the US06 driving cycle, clearly indicating that the equivalent overpotential decreases during operation, so the capacity with the active pressure management strategy is 1.47% greater than that under passive pressure conditions. In other words, the active pressure management strategy may improve LIB lifespan by mitigating the reversible pressure that affects accumulated stress and fatigue failure. Furthermore, energy consumption (amount of energy) required by the phase transition actuator is 29.89 Wh during this operation, which is 50.97% of energy consumption for a targeted LIB. This would be significant when a single LIB is managed with the proposed active pressure management method. However, one actuator can manage an entire battery module or pack connected in series because the same pressure is transmitted to all LIBs in this configuration with the proposed method (Oh and Epureanu, 2017). In other words, one actuator can manage all cells in the configuration of series connection in a module and pack condition, suggesting that implementing this method to a module and pack is economical. The larger connection of LIBs in series, the more efficient pressure management would be expected. Specifically, a battery pack in the Ford Fusion hybrid electric vehicle comprises 38 LIBs connected in series (Oh and Epureanu, 2017). In this configuration, one actuator can be added to manage all of 38 LIBs with the proposed method, suggesting that additional energy consumption is only 1.34% of an entire pack.

However, this pressure management performance is relatively weak compared to that under stationary charge and discharge conditions because of the saturation phenomenon of the phase transition actuator at each interval, which is also reflected in the stationary operation at a high C-rate. Specifically, the maximum/minimum current are frequently applied to the phase transition actuator (Fig. 8(c)), suggesting that the compressive pressure required to manage stochastic driving conditions exceeds the limit of the phase transition actuator because the maximum C-rate imposed on the LIB is up to 10 C under harsh stochastic operational conditions. Specifically, the maximum pressure variation estimated by the proposed controller is 33.1 Pa in one interval, which is twice the limit of the average pressure variation of the actuator. Therefore, the saturation phenomena of the phase transition actuator result in limited pressure management capabilities, suggesting that a greater capacity for the phase transition actuator may an alternative solution.

Degradation phenomena of the actuator should also be considered for real-world applications because the entire lifetime of the LIB modules and packs depends on the lifetime of the actuator when implementing the proposed method to a module and pack. To mitigate degradation of the phase transition actuator, the larger capacity of a LIB compared to a targeted LIB can be used for the actuator because the usage of a small SOC region would prolong the lifetime of the phase transition actuator (Wikner et al., 2021). The secondary phase transition actuator can also be added in series in module and pack configurations and then this actuator can be used when the first phase transition actuator cannot play its role because of significant degradation. This method is feasible because the calendar life of LIBs is longer than the cycle life of LIBs (Ecker et al., 2014). Future work should consider these aspects for real-world applications of the proposed method.

5. Conclusions

This study proposed a novel active pressure management method for LIBs in module or pack conditions using a closed-loop control method and phase transition actuator. The proposed method can manage the compressive pressure imposed on an LIB to ensure an optimal state by compensating the reversible and irreversible pressure during operation. Measurements of the capacity and equivalent impedance of an LIB under various pressure conditions reveal that LIB performance and characteristics significantly depend on compressive pressure, indicating that the LIB could be maintained at an optimal pressure level through the proposed method. Furthermore, active pressure management in the US06 driving cycle demonstrated that the proposed method can be effectively used in real-world applications. Notably, the remaining discharge capacity increased by 1.47% compared to that under passive pressurized conditions. This improvement is significant from a degradation perspective. Future work include determining the optimal pressure to mitigate concerns regarding degradation, executing pressure management with the setpoint of the optimal pressure, and thereby demonstrating the lifespan improvement of LIBs in a long-term degradation experiment. Furthermore, elaborate pressure management strategies with a larger capacity actuator should be established to enhance the performances of the proposed method.

CRediT authorship contribution statement

Jinho Jeong: Methodology, Conceptualization, Formal analysis, Writing – original draft preparation, Writing – reviewing & editing. **Eunji Kwak:** Validation, Investigation. **Jun-hyeong Kim:** Data curation, Software. **Ki-Yong Oh:** Conceptualization, Formal analysis, Writing – reviewing & editing, Funding acquisition, Supervision, Project administration.

Declaration of competing interest

The authors declare that they have no known competing financial interests or personal relationships that could have appeared to influence the work reported in this paper.

Data availability

Data will be made available on request.

Funding

This work was supported by the Research and Development on Fire Safety Technology for ESS Hydrogen Facilities, 20011568, Development of Automatic Extinguishing System for ESS Fire, funded by the National Fire Agency (NFA, Korea), and the National Research Foundation of Korea (NRF) grant funded by the Korean government (MSIT) (No. 2020R1C1C1003829).

References

Barai, A., Guo, Y., McGordon, A., Jennings, P., 2013. A study of the effects of external pressure on the electrical performance of a lithium-ion pouch cell. In: International Conference on Connected Vehicles and Expo (ICCVE). pp. 295–299.

Barai, A., Tangirala, R., Uddin, K., Chevalier, J., Guo, Y., McGordon, A., Jennings, P., 2017. The effect of external compressive loads on the cycle lifetime of lithium-ion pouch cells. J. Energy Storage 13, 211–219. http://dx.doi.org/10.1016/j.est.2017.07.021.

Beirão, M.D., Maria do Rosário, A.C., Pombo, J.A., Mariano, S.J., 2016. Balancing management system for improving li-ion batteries capacity usage and lifespan. In: 16th International Conference on Environment and Electrical Engineering (EEEIC). IEEE Publications, pp. 1–6.

Berckmans, G., De Sutter, L., Marinaro, M., Smekens, J., Jaguemont, J., Wohlfahrt-Mehrens, M., van Mierlo, J., Omar, N., 2019. Analysis of the effect of applying external mechanical pressure on next generation silicon alloy lithium-ion cells. Electrochim. Acta 306, 387–395. http://dx.doi.org/10.1016/j.electacta.2019.03.138.

Bitzer, B., Gruhle, A., 2014. A new method for detecting lithium plating by measuring the cell thickness. J. Power Sources 262, 297–302. http://dx.doi.org/10.1016/j.jpowsour.2014.03.142.

Cannarella, J., Arnold, C.B., 2014a. State of health and charge measurements in lithium-ion batteries using mechanical stress. J. Power Sources 269, 7–14. http://dx.doi.org/10.1016/j.jpowsour.2014.07.003.

Cannarella, J., Arnold, C.B., 2014b. Stress evolution and capacity fade in constrained lithium-ion pouch cells. J. Power Sources 245, 745–751. http://dx.doi.org/10.1016/j.jpowsour.2013.06.165.

Costa, C.M., Merazzo, K.J., Gonçalves, R., Amos, C., Lanceros-Méndez, S., 2021. Magnetically active lithium-ion batteries towards battery performance improvement. IScience 24, 102691. http://dx.doi.org/10.1016/j.isci.2021.102691.

Deich, T., Hahn, S.L., Both, S., Birke, K.P., Bund, A., 2020. Validation of an actively-controlled pneumatic press to simulate automotive module stiffness for mechanically representative lithium-ion cell aging. J. Energy Storage 28, 101192. http://dx.doi.org/10.1016/j.est.2020.101192.

Dsoke, S., Tian, X., Täubert, C., Schlüter, S., Wohlfahrt-Mehrens, M., 2013. Strategies to reduce the resistance sources on electrochemical double layer capacitor electrodes. J. Power Sources 238, 422–429. http://dx.doi.org/10.1016/j.jpowsour.2013.04.031.

Ecker, M., Nieto, N., Käbitz, S., Schmalstieg, J., Blanke, H., Warnecke, A., Sauer, D.U., 2014. Calendar and cycle life study of Li (NiMnCo) O2-based 18650 lithium-ion batteries. J. Power Sources 248, 839–851. http://dx.doi.org/10.1016/j.jpowsour.2013.09.143.

Fang, C.C., Lu, B.Y., Pawar, G., Zhang, M.H., Cheng, D.Y., Chen, S.R., Ceja, M., Doux, J.M., Musrock, H., Cai, M., Liaw, B., Meng, Y.S., 2021. Pressure-tailored lithium deposition and dissolution in lithium metal batteries. Nat. Energy 6, 987–994. http://dx.doi.org/10.1038/s41560-021-00917-3.

Hahn, S., Theil, S., Kroggel, J., Birke, K.P., 2021. Pressure prediction modeling and validation for lithium-ion pouch cells in buffered module assemblies. J. Energy Storage 40, 102517. http://dx.doi.org/10.1016/j.est.2021.102517.

Jalkanen, K., Karppinen, J., Skogström, L., Laurila, T., Nisula, M., Vuorilehto, K., 2015. Cycle aging of commercial NMC/graphite pouch cells at different temperatures. Appl. Energy 154, 160–172. http://dx.doi.org/10.1016/j.apenergy.2015.04.110.

Kaasik, F., Tamm, T., Hantel, M.M., Perre, E., Aabloo, A., Lust, E., Bazant, M.Z., Presser, V., 2013. Anisometric charge dependent swelling of porous carbon in an ionic liquid. Electrochem. Commun. 34, 196–199. http://dx.doi.org/10.1016/j.elecom.2013.06.011.

Käbitz, S., Gerschler, J.B., Ecker, M., Yurdagel, Y., Emmermacher, B., André, D., Mitsch, T., Sauer, D.U., 2013. Cycle and calendar life study of a graphite | LiNi1/3Mn1/3Co1/3O2 li-ion high energy system. Part A: Full cell characterization. J. Power Sources 239, 572–583. http://dx.doi.org/10.1016/j.jpowsour.2013.03.045.

Keil, P., Jossen, A., 2016. Charging protocols for lithium-ion batteries and their impact on cycle life–an experimental study with different 18650 high-power cells. J. Energy Storage 6, 125–141. http://dx.doi.org/10.1016/j.est.2016.02.005.

Kim, J.H., Kwak, E., Oh, K.Y., 2021. Degradation pathways dependency of a lithium iron phosphate battery on temperature and compressive force. Int. J. Energy Res. 45, 6888–6906. http://dx.doi.org/10.1002/er.6280.

Kim, S.U., Monroe, C.W., 2013. Increasing the rate capability of batteries with electrolyte flow. Appl. Energy 103, 207–211. http://dx.doi.org/10.1016/j.apenergy.2012.09.028.

Kim, J., Oh, J., Lee, H., 2019. Review on battery thermal management system for electric vehicles. Appl. Therm. Eng. 149, 192–212.

Kotak, N., Barai, P., Verma, A., Mistry, A., Mukherjee, P.P., 2018. Electrochemistry-mechanics coupling in intercalation electrodes. J. Electrochem. Soc. 165, A1064. http://dx.doi.org/10.1149/2.0621805jes.

Kwak, E., Jeong, S., Kim, J.H., Oh, K.Y., 2021. Prediction of compression force evolution over degradation for a lithium-ion battery. J. Power Sources 483, 229079. http://dx.doi.org/10.1016/j.jpowsour.2020.229079.

Kwak, E., Son, D.S., Jeong, S., Oh, K.Y., 2020. Characterization of the mechanical responses of a LiFePO4 battery under different operating conditions. J. Energy Storage 28, 101269. http://dx.doi.org/10.1016/j.est.2020.101269.

Lee, J.H., Lee, H.M., Ahn, S., 2003. Battery dimensional changes occurring during charge/discharge cycles - thin rectangular lithium ion and polymer cells. J. Power Sources 119–121, 833–837. http://dx.doi.org/10.1016/S0378-7753(03)00281-7.

Louli, A.J., Ellis, L.D., Dahn, J.R., 2019. Operando pressure measurements reveal solid electrolyte interphase growth to rank Li-ion cell performance. Joule 3, 745–761. http://dx.doi.org/10.1016/j.joule.2018.12.009.

Manthiram, A., 2011. Materials challenges and opportunities of lithium ion batteries. J. Phys. Chem. Lett. 2, 176–184. http://dx.doi.org/10.1021/jz1015422.

Mukhopadhyay, A., Tokranov, A., Xiao, X., Sheldon, B.W., 2012. Stress development due to surface processes in graphite electrodes for li-ion batteries: A first report. Electrochim. Acta 66, 28–37. http://dx.doi.org/10.1016/j.electacta.2012.01.058.

Müller, V., Scurtu, R.-G., Memm, M., Danzer, M.A., Wohlfahrt-Mehrens, M., 2019a. Study of the influence of mechanical pressure on the performance and aging of lithium-ion battery cells. J. Power Sources 440, http://dx.doi.org/10.1016/j.jpowsour.2019.227148,227148.

Müller, V., Scurtu, R.-G., Richter, K., Waldmann, T., Memm, M., Danzer, M.A., Wohlfahrt-Mehrens, M., 2019b. Effects of mechanical compression on the aging and the expansion behavior of Si/C-composite | NMC811 in different lithium-ion battery cell formats. J. Electrochem. Soc. 166, A3796–A3805. http://dx.doi.org/10.1149/2.1121915jes.

Mussa, A.S., Klett, M., Lindbergh, G., Lindström, R.W., 2018. Effects of external pressure on the performance and ageing of single-layer lithium-ion pouch cells. J. Power Sources 385, 18–26. http://dx.doi.org/10.1016/j.jpowsour.2018.03.020.

Oh, K.-Y., Epureanu, B.I., 2017. A phenomenological force model of Li-ion battery packs for enhanced performance and health management. J. Power Sources 365, 220–229. http://dx.doi.org/10.1016/j.jpowsour.2017.08.058.

Oh, K.-Y., Epureanu, B.I., Siegel, J.B., Stefanopoulou, A.G., 2016. Phenomenological force and swelling models for rechargeable lithium-ion battery cells. J. Power Sources 310, 118–129. http://dx.doi.org/10.1016/j.jpowsour.2016.01.103.

Oh, K.-Y., Siegel, J.B., Secondo, L., Kim, S.U., Samad, N.A., Qin, J., Anderson, D., Garikipati, K., Knobloch, A., Epureanu, B.I., Monroe, C.W., Stefanopoulou, A., 2014. Rate dependence of swelling in lithium-ion cells. J. Power Sources 267, 197–202. http://dx.doi.org/10.1016/j.jpowsour.2014.05.039.

Ohzuku, T., Iwakoshi, Y., Sawai, K., 1993. Formation of lithium-graphite intercalation compounds in nonaqueous electrolytes and their application as a negative electrode for a lithium ion (shuttlecock) cell. J. Electrochem. Soc. 140, 2490–2498. http://dx.doi.org/10.1149/1.2220849.

Ovejas, V.J., Cuadras, A., 2019. Effects of cycling on lithium-ion battery hysteresis and overvoltage. Sci. Rep. 9, 14875. http://dx.doi.org/10.1038/s41598-019-51474-5.

Pastor-Fernández, C., Uddin, K., Chouchelamane, G.H., Widanage, W.D., Marco, J., 2017. A comparison between electrochemical impedance spectroscopy and incremental capacity-differential voltage as Li-ion diagnostic techniques to identify and quantify the effects of degradation modes within battery management systems. J. Power Sources 360, 301–318. http://dx.doi.org/10.1016/j.jpowsour.2017.03.042.

Peabody, C., Arnold, C.B., 2011. The role of mechanically induced separator creep in lithium-ion battery capacity fade. J. Power Sources 196, 8147–8153. http://dx.doi.org/10.1016/j.jpowsour.2011.05.023.

Scrosati, B., Garche, J., 2010. Lithium batteries: Status, prospects and future. J. Power Sources 195, 2419–2430. http://dx.doi.org/10.1016/j.jpowsour.2009.11.048.

Sethuraman, V.A., Chon, M.J., Shimshak, M., Srinivasan, V., Guduru, P.R., 2010. In situ measurements of stress evolution in silicon thin films during electrochemical lithiation and delithiation. J. Power Sources 195, 5062–5066. http://dx.doi.org/10.1016/j.jpowsour.2010.02.013.

Sethuraman, V.A., Van Winkle, N., Abraham, D.P., Bower, A.F., Guduru, P.R., 2012. Real-time stress measurements in lithium-ion battery negative-electrodes. J. Power Sources 206, 334–342. http://dx.doi.org/10.1016/j.jpowsour.2012.01.036.

Shen, X., Zhang, R., Shi, P., Chen, X., Zhang, Q., 2021. How does external pressure shape Li dendrites in Li metal batteries? Adv. Energy Mater. 11, 2003416. http://dx.doi.org/10.1002/aenm.202003416.

Shi, D., Xiao, X., Huang, X., Kia, H., 2011. Modeling stresses in the separator of a pouch lithium-ion cell. J. Power Sources 196, 8129–8139. http://dx.doi.org/10.1016/j.jpowsour.2011.05.026.

Siegel, J.B., Stefanopoulou, A.G., Hagans, P., Ding, Y., Gorsich, D., 2013. Expansion of lithium ion pouch cell batteries: Observations from neutron imaging. J. Electrochem. Soc. 160, A1031–A1038. http://dx.doi.org/10.1149/2.011308jes.

Sihvo, J., Roinila, T., Stroe, D.-I., 2020. Novel fitting algorithm for parametrization of equivalent circuit model of Li-ion battery from broadband impedance measurements. IEEE Trans. Ind. Electron. 68, 4916–4926. http://dx.doi.org/10.1109/TIE.2020.2988235.

Tianze, L., Xia, Z., Chuan, J., Luan, H., 2009. Analysis of the characteristics of piezoelectric sensor and research of its application. In: 18th IEEE International Symposium on the Applications of Ferroelectrics. pp. 1–4.

US Environmental Protection Agency (EPA), 2006. http://www.epa.gov/otaq/emisslab/methods.

Vetter, J., Novák, P., Wagner, M.R., Veit, C., Möller, K.-C., Besenhard, J., Winter, M., Wohlfahrt-Mehrens, M., Vogler, C., Hammouche, A., 2005. Ageing mechanisms in lithium-ion batteries. J. Power Sources 147, 269–281. http://dx.doi.org/10.1016/j.jpowsour.2005.01.006.

Waldmann, T., Wilka, M., Kasper, M., Fleischhammer, M., Wohlfahrt-Mehrens, M., 2014. Temperature dependent ageing mechanisms in lithium-ion batteries – A post-mortem study. J. Power Sources 262, 129–135. http://dx.doi.org/10.1016/j.jpowsour.2014.03.112.

Wang, H., Ma, L., 2017. Thermal management of a large prismatic battery pack based on reciprocating flow and active control. Int. J. Heat Mass Transfer 115, 296–303.

Wang, X., Sone, Y., Segami, G., Naito, H., Yamada, C., Kibe, K., 2007. Understanding volume change in lithium-ion cells during charging and discharging using in situ measurements. J. Electrochem. Soc. 154, A14. http://dx.doi.org/10.1149/1.2386933.

Wikner, E., Björklund, E., Fridner, J., Brandell, D., Thiringer, T., 2021. How the utilised SOC window in commercial li-ion pouch cells influence battery ageing. J. Power Sources Adv. 8, 100054. http://dx.doi.org/10.1016/j.powera.2021.100054.

Williard, N., Hendricks, C., Chung, J., Pecht, M., 2021. Effects of external pressure on phase stability and diffusion rate in lithium-ion cells. J. Electroanal. Chem. 895, 115400. http://dx.doi.org/10.1016/j.jelechem.2021.115400.

Wu, W., Wang, S., Wu, W., Chen, K., Hong, S., Lai, Y., 2019. A critical review of battery thermal performance and liquid based battery thermal management. Energy Convers. Manage. 182, 262–281.D.

Zhang, X., Jiang, B., Guo, J., Xie, Y., Tang, L., 2014. Large and stable reversible lithium-ion storages from mesoporous SnO2 nanosheets with ultralong lifespan over 1000 cycles. J. Power Sources 268, 365–371. http://dx.doi.org/10.1016/j.jpowsour.2014.06.077.

Zhang, J., Kang, B., Luo, Q., Zou, S., 2020. Effects of pressure evolution on the decrease in the capacity of lithium-ion batteries. Int. J. Electrochem. Sci. 15, 8422–8436. http://dx.doi.org/10.20964/2020.09.71.

Zhang, N., Tang, H., 2012. Dissecting anode swelling in commercial lithium-ion batteries. J. Power Sources 218, 52–55. http://dx.doi.org/10.1016/j.jpowsour.2012.06.071.

Zhang, X., Wang, Q.J., Harrison, K.L., Jungjohann, K., Boyce, B.L., Roberts, S.A., Attia, P.M., Harris, S.J., 2019. Rethinking how external pressure can suppress dendrites in lithium metal batteries. J. Electrochem. Soc. 166, A3639–A3652. http://dx.doi.org/10.1149/2.0701914jes.